Stability and Exfoliation of Germanane: A Germanium Graphane Analogue

Undergraduate Thesis

Presented in Partial Fulfillment of the Requirements for the Degree of Bachelor of Science in Chemistry *with Research Distinction in Chemistry* in the College of Arts and Sciences of The Ohio State University

By

Elisabeth Bianco

The Ohio State University

May 2013

Thesis Committee:

Joshua Goldberger, Advisor

Patrick Woodward

Abstract

Graphene's success has shown that it is not only possible to create stable, single-atom thick sheets from a crystalline solid, but that these materials have fundamentally different properties than the parent material. We have synthesized for the first time, mm-scale crystals of a hydrogen-terminated germanium multilayered graphane analogue (germanane, GeH) from the topochemical deintercalation of $CaGe_2$. This layered van der Waals solid is analogous to multilayered graphane (CH). The surface layer of GeH only slowly oxidizes in air over the span of 5 months, while the underlying layers are resilient to oxidation based on X-ray Photoelectron Spectroscopy (XPS) and Fourier Transform Infrared Spectroscopy (FTIR) measurements. The GeH is thermally stable up to 75 ^{o}C, however, above this temperature amorphization and dehydrogenation begin to occur. These sheets can be mechanically exfoliated as single and few layers onto SiO_2/Si surfaces. This material represents a new class of covalently terminated graphane analogues and has great potential for a wide range of optoelectronic and sensing applications, especially since theory predicts a direct band gap of 1.53 eV and an electron mobility ~five times higher than that of bulk Ge.

Acknowledgements

This work was supported in part by an allocation of computing time from the Ohio Supercomputing Center, as well as the Analytical Surface Facility at OSU chemistry, supported by National Science Foundation under the grant number (CHE-0639163). Thank you to The Ohio State University Undergraduate Instrumental Analysis Program for the use of their instrumentation. This project was supported by the National Science Foundation under project number DMR-1201953, the Army Research Office (W911-NF-12-1-0481), the Center for Emergent Materials at The Ohio State University, a NSF MRSEC at The Ohio State University (Grant DMR-0820414), The Ohio State University Materials Research Seed Grant Program, and startup funding from The Ohio State University.

A special thank you to Oscar Restrepo and Prof. Wolfgang Windl in the Materials Science and Engineering Department at Ohio State for performing the band structure simulations reported herein. Thank you to my labmates, especially Sheneve Butler and ShiShi Jiang, for your contributions to this work. Finally, my deepest gratitude is to my advisor, Prof. Josh Goldberger, for your unwavering support and mentorship.

Vita

Education

B.S., Chemistry ……..The Ohio State University
Cum Laude 2013
with Research Distinction in Chemistry

Publications

1. E. Bianco, S. Butler, S. Jiang, O. Restrepo, W. Windl, J. Goldberger "**Stability and Exfoliation of Germanane: A Germanium Graphane Analogue**" *ACS Nano.* DOI: 10.1021/nn4009406.

Table of Contents

List of Figures

Chapter 1: Synthesis and Characterization of Germanane

1.1 Introduction

The discovery of single-layer graphene has shown that it is not only possible to create stable single-atom thick layers from anisotropic crystal structures held together mainly *via* weak van der Waals interactions, but that these isolated layers can have fundamentally different electronic structures and properties than the parent material.[1,2] For example, in a single layer of graphene electrons behave as massless Dirac fermions, resulting in potential applications for sensors, high mobility transistors, transparent conducting electrodes, and photocatalyst supports.[3-5] This has sparked much recent interest toward understanding how the bulk properties of other layered van der Waals bonded crystal structures (MoS_2, WS_2, Bi_2Se_3, BN, etc…) change when prepared as isolated individual sheets.[6,7] For example, bulk MoS_2 normally has an indirect band gap at 1.29 eV, whereas isolated single layers of MoS_2 have a direct gap (1.8 eV).[8-10] Single layers of MoS_2 have also attracted much interest as high mobility transistors.[10]

Most of the layered materials studied to date are comprised of neutral or ionic layers and lack the possibility for chemical functionalization. Designing electronically active layers that could be covalently modified without disrupting the electronically relevant state would be incredibly advantageous for a wide range of applications. The nature of this terminal substituent would potentially give a synthetic handle for not only tuning the entire electronic structure based off of its identity and electron withdrawing capability, but could also enable the grafting of functional ligands for high-specificity sensing applications. Graphene can be grafted with organic components, oxidized or

even terminated with hydrogen atoms to form graphane (CH);[11,12] however, these modifications disrupt the excellent carrier mobility in graphene, and also are not stable long term.[13] Other Group IV layered lattices, may maintain appreciable conductivity when the atoms are in the sp^3-hybridized state. Recently, single-layer thick sp^2 and sp^3 group IV systems have attracted considerable theoretical and experimental interest.[14-17]

It has been previously shown that layered Zintl phases such as $CaSi_2$ and $CaGe_2$ can be topochemically deintercalated in aqueous HCl at low temperatures to produce layered silicon and germanium solids.[18-20] The resultant four-coordinate puckered lattice of Si and Ge atoms has an analogous geometry to sp^3-hybridized graphane, or a Si/Ge(111) surface in which every Si/Ge atom is terminated with either –H or –OH above or below the layer.[18,21] There is a great propensity for the silicon lattice to oxidize, initially forming siloxene ($SiH_{0.5}(OH)_{0.5}$) sheets that are terminated with either Si–H or Si–OH bonds at the fourth coordination site, which eventually degrade to form SiO_2 under ambient conditions.[20,22] Appreciable Si–OH bond formation is always observed in the FTIR spectrum as an intense, broad Si–O stretching mode at 1000-1200 cm^{-1}, even after HF treatment.[20] In contrast, the air- and thermal-stability of germanane (GeH) has not been rigorously characterized. Resistance to oxidation is an essential prerequisite for many future applications. From previous work,[18] there remain questions about the structure, air-stability, thermal-stability, and crystallinity of bulk GeH, as characterization did not include transmission electron microscopy, Raman spectroscopy, and XPS data. Additionally, while previous work focused on interconverting μm-thick epitaxial thin films of $CaGe_2$ on Ge(111) into GeH, the present

study focuses on the synthesis of free-standing crystals of $CaGe_2$. Furthermore, the exfoliation of single- and few-layer sheets of GeH has yet to be shown.

Herein, we demonstrate for the first time, the gram-scale synthesis of mm-scale crystals of a layered GeH van der Waals solid that have platelet-like morphologies akin to Kish graphite. We prove by FTIR and XPS measurements that the surface layer of GeH slowly oxidizes in air over the span of 5 months while the underlying layers resist oxidation. GeH is thermally stable up to 75 ^{o}C, above which amorphization begins to occur. Amorphization is complete at 175 ^{o}C, and dehydrogenation occurs from 200-250 ^{o}C We show that the layered GeH has an observed band gap at 1.59 eV, and also demonstrate the exfoliation of single and few-layers onto SiO_2 / Si substrates. Finally, we perform high-level theory calculations of the electronic structure that predict the effective masses, mobilities, and band gap of bulk and single layer germanane.

1.2 Synthesis and Structural Characterization

Hydrogen-terminated germanane was synthesized by the topotactic deintercalation of β-$CaGe_2$ in aqueous HCl at -40 ^{o}C for eight days (**Figure 1**). 2-6 mm crystals of β-$CaGe_2$ were first synthesized by sealing stoichiometric ratios of Ca and Ge in a quartz tube, annealed at 950 ^{o}C, and cooled down over a period of 2-10 days (**Figure 1b**). The purity of $CaGe_2$ was confirmed *via* powder X-ray diffraction (**Figure 1d**). After HCl treatment, the product was filtered and washed with distilled water and methanol to remove residual $CaCl_2$, yielding crystallites of GeH that are 2-3 mm in diameter and < 100 μm in thickness (**Figure 1c**). By X-ray diffraction analysis, GeH can be fit to a

hexagonal unit cell with 2 layers per *c*-unit cell spacing with lattice parameters: *a* = 3.880 Å and *c* = 11.04 Å (5.5 Å per layer). Compared to the original $CaGe_2$ unit cell parameters of *a* = 3.987 Å, *c* = 30.0582 Å, (6 layer stacking, *c*/6 = 5.097 Å) the hydrogen-terminated germanane is slightly contracted in the *a* direction but expanded in the *c*-direction due to the replacement of Ca^{2+} with 2 Ge–H bonds between each layer. These lattice parameters do not correspond to any of the previously reported allotropes of germanium.[23,24] The narrower full-width-half-maximum (FWHM) of the (100) and (110) diffraction reflections (~0.4 $^{o}2\theta$) compared to the (002), (011) and (112) peaks (~1.3 $^{o}2\theta$) indicates that there is significant inconsistency in the interlayer spacing along the *c* axis. This disorder along the *c* axis precludes further structure determination *via* Rietveld analysis.

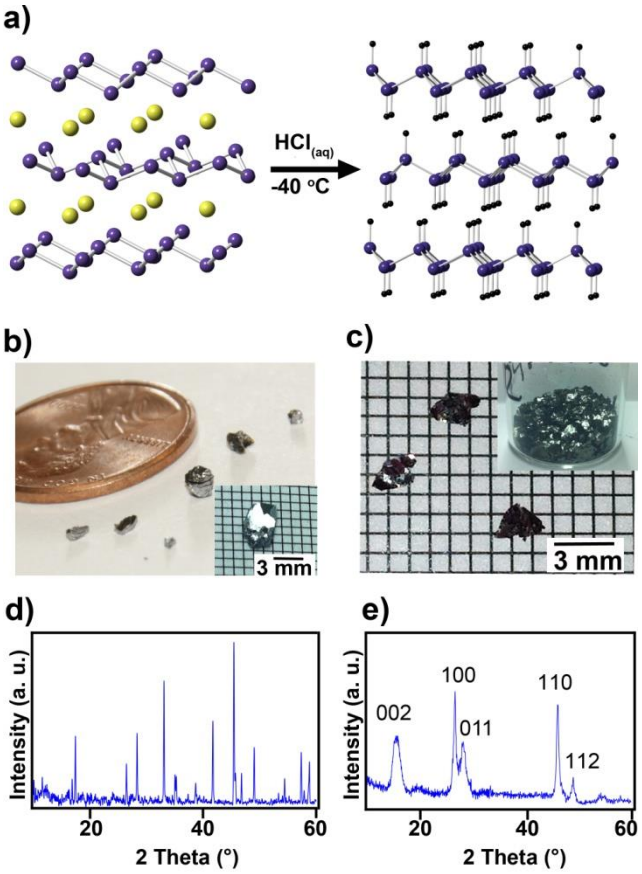

Figure 1. a) Schematic illustration of topotactic deintercalation of $CaGe_2$ to GeH. Optical images of b) $CaGe_2$ and c) GeH crystals with select crystals on graph paper with a 1 mm grid (inset). Powder XRD pattern of d) $CaGe_2$ and e) GeH.

Transmission electron microscopy analysis indicates the product has a layered morphology with individual layers having less contrast than the 10 nm lacey carbon support grid (**Figure 2a,b**). The energy dispersive X-ray spectrum has a strong Ge signal, and an absence of Ca and O signals. A trace amounts of Cl is present, and the Cl:Ge ratio was estimated to be 2:98 (**Figure 2d**). **Figure 2c** is an electron diffraction pattern taken orthogonal to the layers, showing a hexagonal arrangement of diffraction peaks that occur in the *a* and *b* directions. This data further confirms that the crystallinity

of the germanium layered framework is preserved upon HCl treatment, and there is a strong registration in the stacking between each layer. The GeH electron diffraction pattern can be indexed to a simple hexagonal unit cell with $a = b \approx 3.87$ Å, assuming a [001] zone axis.

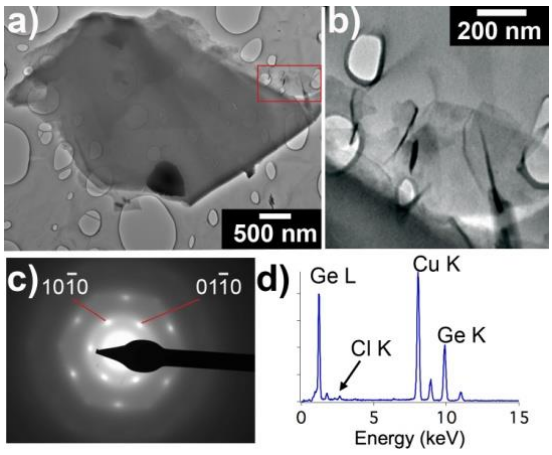

Figure 2. a) Low magnification and b) Magnified TEM micrograph of GeH platelets c) Electron diffraction pattern of platelets collected down the 0001 zone axis. d) Energy dispersive X-ray Spectroscopy of the GeH sheets.

To further confirm hydrogen termination, we performed FTIR, Raman spectroscopy, and X-ray photoelectron spectroscopy (XPS) on the germanane product (**Figure 4a**). Transmission mode FTIR of samples ground up and pressed into KBr pellets show extremely strong Ge—H stretching and multiple wagging modes at ~2000 cm^{-1} and 570, 507, and 475 cm^{-1}, respectively. Additionally, weak vibrational modes at 770 cm^{-1} and 825 cm^{-1} are also observed. These two vibrations also occur in the spectra of amorphous $Ge_{0.7}$:$H_{0.3}$ thin films, and have been assigned by M. Cardona *et al.* to originate from bond-bending Ge—H_2 modes from nearest neighbor Ge atoms.[25,26] Thus, we hypothesize that these vibrations correspond to Ge—H_2 bond bending modes from

neighboring Ge atoms at the edges of each crystalline germanane sheet, and/or to Ge—H_2 bonds within the lattice arising from Ge vacancies. We do not observe the presence of the broad, intense Ge—O—Ge and Ge—O vibrational modes that occur between 800 cm^{-1} and 1000 cm^{-1}.[27] To confirm that these vibrational modes originate from Ge—H_2 and not Ge—O—Ge, we prepared GeD by treating $CaGe_2$ in 95% deuterated DCl/D_2O, and collected the FTIR spectrum (**Figure 3**). The 825 and 770 cm^{-1} vibrational modes almost completely disappear, and new Ge—D_2 modes at 586 cm^{-1} and 514 cm^{-1} appear along with residual Ge-H wagging modes. This is generally consistent with the change in reduced mass upon deuteration, and these vibrational frequencies are also apparent in amorphous $Ge_{0.7}$:$D_{0.3}$ films.[25]

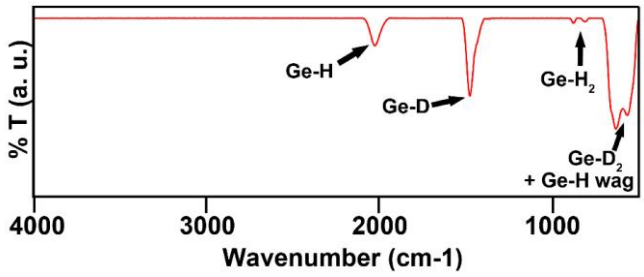

Figure 3. Mid-FTIR spectrum of GeD.

From Raman spectroscopy (**Figure 4b**), the main Ge—Ge stretch in GeH occurs at 302 cm^{-1} which is slightly blue-shifted compared to the 297 cm^{-1} E_2 Raman mode for crystalline germanium. In addition, a second vibrational mode emerges at 228 cm^{-1}. We performed *ab initio* calculations of the Γ-point phonon modes in GeH using Perdew-Burke-Ernzerhof (PBE) functionals as implemented in VASP.[27,28] These calculations

predict the presence of Ge-based A_1 and E_2 Raman modes (assuming a C_{6v} point group) that occur at 223 cm^{-1} and 289 cm^{-1}, respectively, which are in good agreement with the observed Raman modes. The symmetries of the vibrational modes are shown in the **Figure 4b** inset.

XPS measurements are also indicative of a single germanium oxidation state. XPS Analysis of the Ge *2p3/2* peak for GeH shows a single peak at 1217.8 eV, which is indicative of Ge^{+1}. A shift in the Ge *2p3/2* peak energy from Ge^0 (1217.0 eV) is expected since hydrogen is more electronegative than germanium (**Figure 4c**). A control Ge(111) wafer with surface oxide shows a mixture of germanium oxidation states ranging from Ge^0 (1217.0 eV) to Ge^{2+} (1218.9 eV) to Ge^{4+} (1221.4 eV).

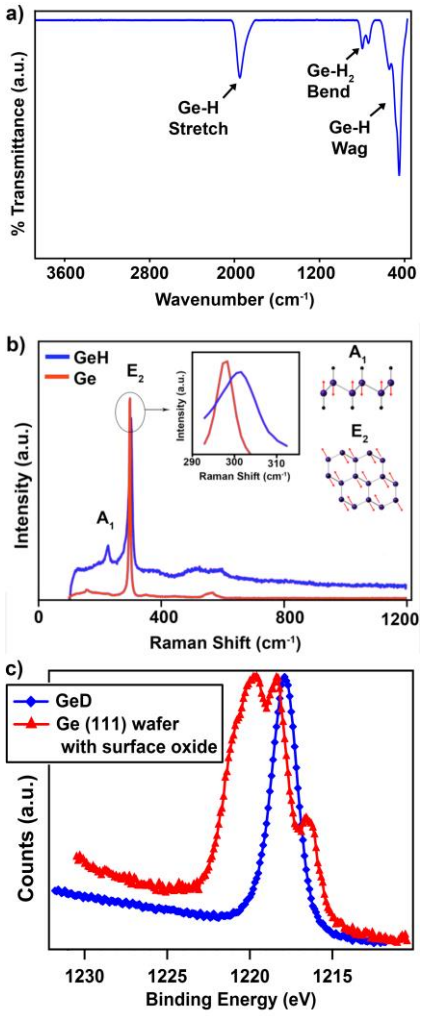

Figure 4. a) Transmission-mode FTIR of GeH. b) Raman spectrum of GeH (red) and Ge powder (blue), highlighting the difference in energy of the E_2 peak between GeH and Ge (middle inset), as well as a schematic illustration of the A_1 and E_2 vibrational modes. c) XPS spectrum of the Ge *2p* peak for GeH and a Ge(111) wafer with native surface oxide.

Chapter 2: Air-Stability

The potential utility of germanane for any optoelectronic or sensing device strongly hinges on its air and temperature stability. Some previous reports state that hydrogen-terminated Ge(111) surfaces having the same atomic configuration as GeH are resistant to oxidation when the Ge surface has minimal defects, although some debate remains.[27-29] Because FTIR spectroscopy is an extremely sensitive probe of the presence of Ge—O and Ge—H bonds, we conducted a time-dependent FTIR study to determine if Ge—O vibrational modes in the 800-1000 cm^{-1} range emerge after exposure to an ambient atmosphere. After 60 days we observed virtually no change in this range, thus proving that the bulk of GeH resists oxidation (**Figure 5a**). Additionally, time dependent XPS was performed to probe changes in the Ge oxidation state of the surface after exposing these layered GeH crystals to air (**Figure 5b**), and the percentage of each germanium oxidation state for all spectra was calculated by applying a standard Gaussian fit. After 1 month of exposure to air, a $Ge^{2+/3+}$ shoulder emerges at ~1219.3 eV (19.5% $Ge^{2+/3+}$). This peak becomes more intense after 5 months of air exposure (29.7% $Ge^{2+/3+}$). After Ar etching the top 0.5 nm (<1 layer), the $Ge^{2+/3+}$ almost completely disappears with 10.1% $Ge^{2+/3+}$ remaining. Together, the XPS and FTIR suggest that only the surface becomes oxidized over time.

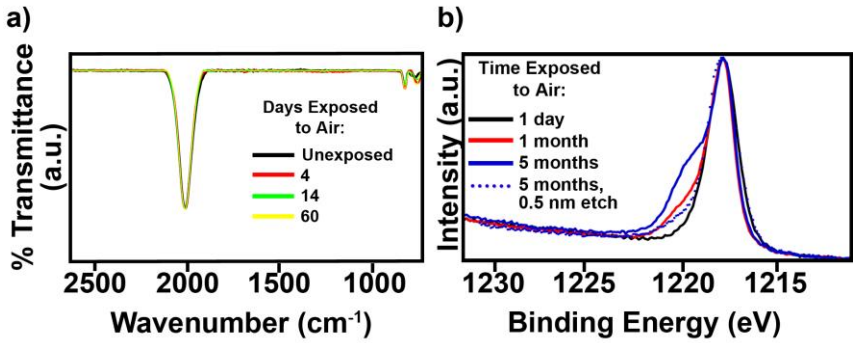

Figure 5. a) Time dependent reflection mode FTIR of a GeH platelet after exposure to ambient atmosphere for up to 60 days, collected *via* reflection mode, highlighting minimal changes in the relative intensity of the Ge–H to Ge–O vibrations. b) Time dependent XPS spectra of germanane immediately after exposure to atmosphere, after 1 day, and 5 months, followed by Ar etching by 0.5 nm.

Chapter 3: Optical Properties

The optical properties of germanane were investigated by diffuse reflectance absorption (DRA) spectroscopy. The silver-black material has a broad absorption over visible wavelengths and a linear approximation of the absorption edge suggests a band gap of approximately 1.59 eV (**Figure 6a)**. The Tauc/Davis-Mott expression for materials with 2D densities of states predicts that the absorbance A($\hbar\omega$) at photon energy $\hbar\omega$ near the band edge would be a step function with a discontinuity in absorbance at the band gap if the band gap was direct allowed. If the band gap was indirect allowed, the absorbance would be proportional to ($\hbar\omega - E_g' \pm E_p$) where E_g' is the indirect gap, and E_p is the energy of a particular phonon mode. However, it has been experimentally established that the Tauc/Davis-Mott approximations of absorption can not unambiguously determine the transition mechanism for fundamental absorption for bulk materials with 2D densities of states.[9,30,31] We modeled the absorbance assuming direct-allowed, direct-forbidden, indirect-allowed and indirect-forbidden gaps using both 2D and 3D densities of states (**Figure 7**). All of these plots estimated fundamental gaps ranging from 1.48 to 1.60 eV. These analyses are complicated by a broad Urbach edge at the lower end of the absorption tail, which is often indicative of a large doping concentration or disorder. The presence of photoluminescence is often a stronger test of a direct band gap. Previously reported studies of GeH thin films proposed that GeH is a direct band gap material with a fundamental absorption gap at 1.8 eV based off of photothermal deflection spectroscopy and photoluminescence that occurs at 0.45 eV

lower, or 1.35 eV.[32] We did not observe any photoluminescence from 1.1-1.8 eV when exciting from 1.38-1.96 eV at temperatures ranging from 14-300 K. This lack of photoluminescence and linear slope in our samples might suggest that germanane has an indirect band gap. However, the lack of photoluminescence alone is not sufficient evidence of an indirect gap. A direct band gap material could lack photoluminescence if there is a large concentration of nonradiative defect states or impurities in the sample, or if the material possesses unique surface or edge states. The presence of any of these can quench photoluminescence and also contribute to the observed bowed Urbach edge. Therefore, further optimization of the growth and etching chemistry will be necessary before dismissing the potential existence of a direct band gap. Also, we propose that more direct measurements, such as angle-resolved photoemission spectroscopy, as well as additional temperature-dependent absorption studies are necessary to completely conclude whether germanane has a direct or indirect band gap, especially since our theory predicts GeH to have a direct band gap.

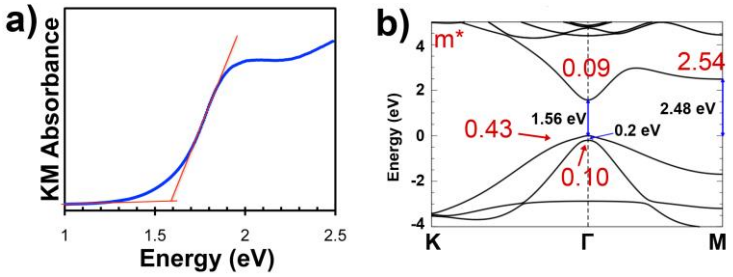

Figure 6. a) DRA spectrum of GeH plotted as (hνα) *vs*. photon energy highlighting a 1.59 eV band gap. The large tail at lower energies b) Electronic band structure of an isolated single layer of GeH calculated using HSE-06 theory including spin-orbit coupling predicting a 1.56 eV direct band gap. The hole and electron effective masses for each extrema are indicated in red.

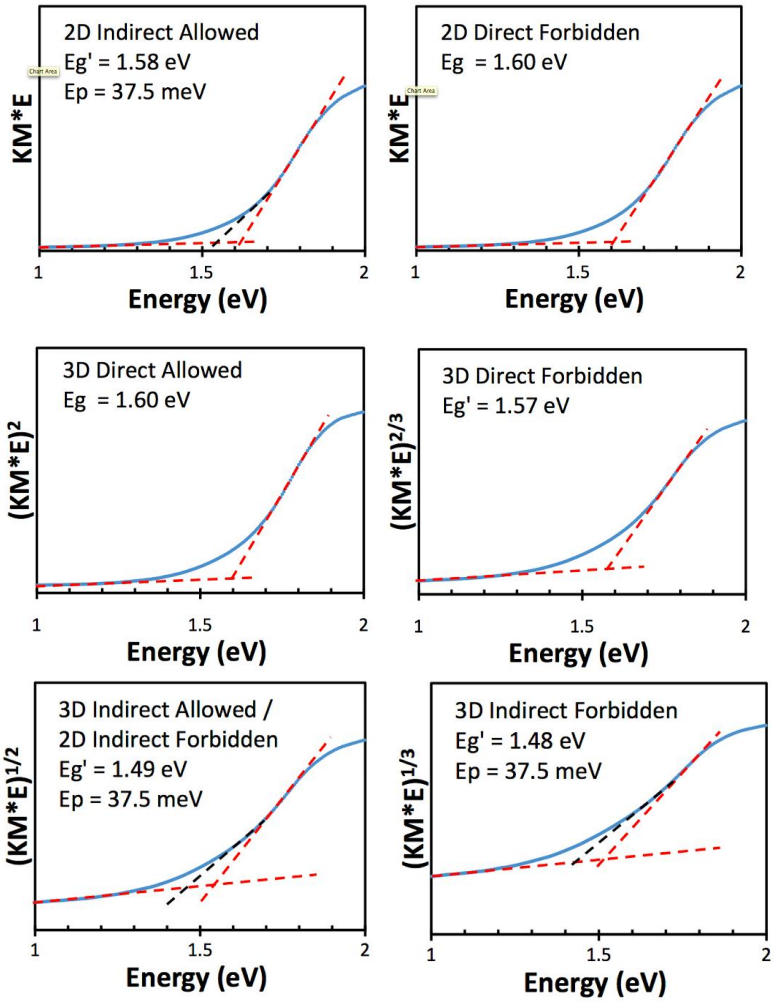

Figure 7. Fits of the absorption spectrum of unannealled GeH to different band structures, according to Tauc/Davis-Mott expressions of 2D densities of states and 3D densities of states. A 37.5 phonon vibration (deduced *via* the 300 cm^{-1} Raman shift) was determined.

Chapter 4: Thermal Stability

The temperature stability of germanane was also probed *via* thermogravimetric analysis (TGA), DRA, XRD, and Raman upon annealing for four hours at a range of temperatures in 5% H_2/Ar. TGA shows a ~1.1% mass loss at 200-250 ºC which is close to the expected mass loss of 1 equivalent of Hydrogen in GeH, as well as a 1.7% mass loss of that occurs between 320-355 ºC (**Figure 8a**). This second mass loss likely corresponds to the loss of Cl (3.6% molar). X-ray fluorescence analysis further supports this, as there is approximately a one order of magnitude decrease in the chlorine intensity from after annealing at 375 ºC. Furthermore, it has been reported in previous temperature programmed desorption studies that Cl desorbs off of germanium at temperatures ranging from 300-350 ºC.[33] However, there is a significant change in the absorption spectrum when annealing at temperatures above 75 ºC. The absorption onset, as detected by DRA, red shifts by 0.06 eV upon annealing at 75 ºC (**Figure 8b**). The absorption profile continues to red-shift with higher temperature annealing until 250 ºC when the absorption onset (0.58 eV) goes below that of bulk germanium (0.67). Previously studies have reported that amorphous Ge thin films have band gaps lower than that of bulk germanium (0.50 *vs*. 0.67 eV)[34] and amorphous hydrogenated germanium films have larger band gaps (1.1 eV).[35] There is no obvious change in the XRD patterns (**Figure 8c**) until 150 ºC, at which point the *c* axis decreases from *c* = 11.04 Å to *c* = 10.70 Å and the FWHM of this 002 reflection decreases from 1.3º 2θ to 0.8º 2θ. The diffraction pattern shows complete amorphization upon annealing at 175

°C. Raman spectroscopy shows a consistent decrease in the intensity of both the Ge—Ge and Ge—H modes as a function of annealing temperature (**Figure 8d**). After 175 °C, there is ~2 order magnitude decrease in the Raman scattering intensity of both the E_2 and A_1 modes. Taken together, this suggests that amorphization occurs at temperatures well below that of dehydrogenation (200-250 °C).

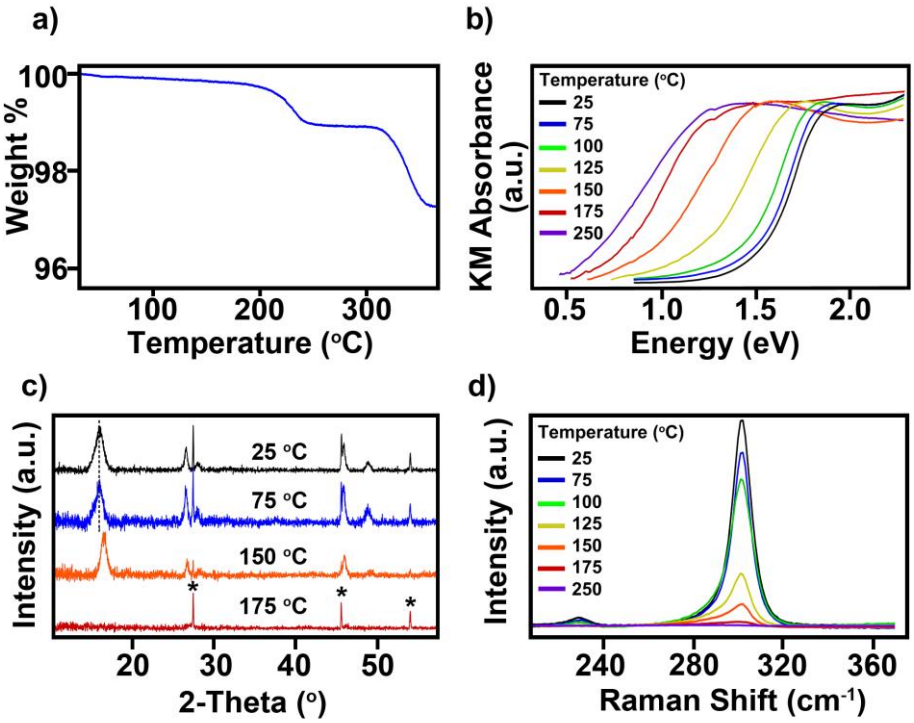

Figure 8. a) TGA analysis of GeH. b) DRA spectra, c) XRD patterns and d) Raman spectra of GeH measured after four hour annealing treatments at various temperatures in 5% H_2 / Ar. In c) the starred peaks correspond to reflections of an internal Ge standard, and the dashed line is drawn to guide the eye.

It was hypothesized that the low-temperature amorphization, the broadness of the 00l reflections, and the lack of observed PL are consequences of the presence of trace percentages of Ge-Cl bonds. If regions with a high concentration of Ge-Cl bonds

amorphize first, this would explain the observed decrease in the *c*-parameter and FWHM of the 00*l* reflections at 150 ºC. The observed diffraction pattern at this temperature is indicative of local domains of pure GeH that did not undergo amorphization due to the lack of nearby chlorine. Though pair distribution function (PDF) measurements will be required to fully dismiss this hypothesis, preliminary experiments were conducted synthesizing germanane using HBr and HI (rather than HCl). If the larger conjugate base had lower propensity to become trapped in the interlayer spacing, and Ge-Cl bonds were in fact the reason for low-temperature amorphization, significant changes in the DRA UV-Vis and Raman spectra would be evident after annealing the material synthesized in HBr and/or HI. This, however, was not the case. After annealing for four hours in 5% H_2/Ar at various temperatures, the absorbance spectra show a similar red-shift trend as a function of temperature and no significant improvement in thermal stability at temperatures between 75 °C and 100 °C (**Figure 9a**). Similarly, the Raman spectra for the materials synthesized in HBr and HI show similar amorphization as that synthesized in HCl, as evidenced by the abrupt decrease in the intensity of both A_1 and E_2 modes at temperatures above 100 °C (**Figure 9b**). Furthermore, in both the HBr and HI-prepared GeH, these two Raman modes exhibit the same ~2 order magnitude decrease in scattering intensity after annealing at 175 °C that was present in the HCl-prepared material. Though further work is required, it appears as though the low-temperature amorphization of germanane is inherent, and not a result of trace Ge-Cl bonds in the lattice.

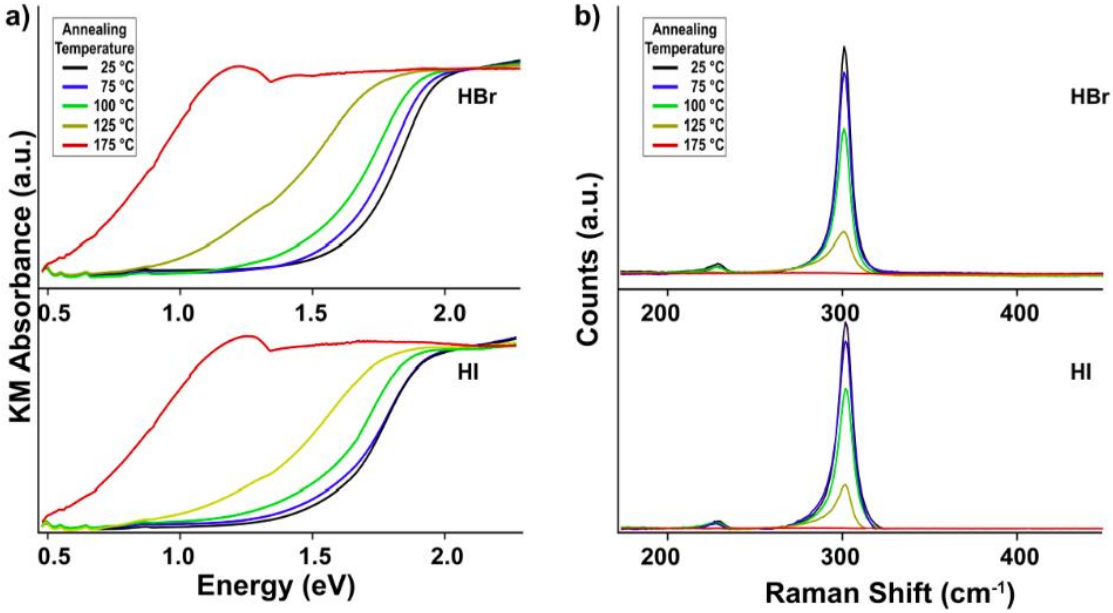

Figure 9. a) DRA and b) Raman spectra of GeH synthesized using HBr, and HI; measured after four hour annealing treatments at various temperatures in 5% H_2/Ar.

Chapter 5: Theoretical Band Structure

Band structure calculations suggest that germanane is a direct band gap material both as isolated layers and in the crystal structure having two layers per unit cell. We used the density functional theory (DFT) code VASP[36,37] to optimize the geometry and calculate the band structure of isolated single layer and 2-layer unit cell GeH. The interactions between cores and electrons were described for relaxation by projector augmented wave (PAW) pseudopotentials[38] within the Perdew-Burke-Ernzerhof (PBE) exchange-correlation function[39,40] with a plane-wave cutoff energy of 600 eV. Van der Waals interactions between the layers were included using the DFT-D2 method by Grimme.[41] For the two-layer structure, the unit cell was modeled as a $P6_3mc$ unit cell with relaxed lattice parameters of a = 4.05 Å, and c = 10.56 Å, thus having a 5.3 Å layer spacing. For the isolated single layer structure, our calculations were performed in a unit cell with 20 Å of additional vacuum between GeH layers. To obtain an accurate description of the band gap in this system, we utilized the hybrid HSE06[42-44] exchange-correlation function. With this function we obtain a direct gap at the Γ point of 1.56 eV for an isolated layer (**Figure 6b**), and 1.53 eV for the 2-layer unit cell (**Figure 10**), which is in excellent agreement with the observed experimental band gap. The calculated band gap for the two layer unit cell at the A point of the Brillouin zone is ~1.77 eV. The difference in energy between the conduction band minimum at the M point and the valence band maximum at Γ is 2.48 eV and 2.33 eV for an isolated layer,

and 2-layer unit cell, respectively. In both cases, spin-orbit splitting at the Γ valence band maximum is 0.2 eV.

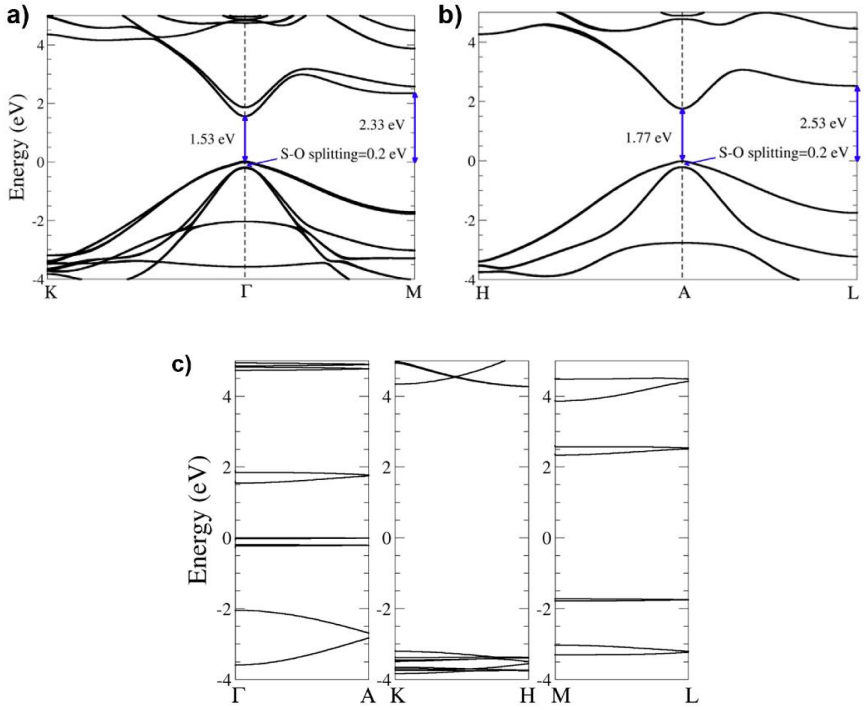

Figure 10. Electronic band structure of 2-layer GeH calculated using HSE-06 theory including spin orbit coupling from a) K-Γ-M, b) H-A-L, and c) Γ-A, K-H, and M-L.

Additionally, the effective masses of the conduction and valence bands at each extremum were calculated for the isolated single layer and are shown in **Figure 6b**. In bulk crystalline germanium, the conduction band minima occur in the 4 equivalent valleys at the L <111> point which have much higher effective mass (m_{eL}* = 1.64) than the conduction band valleys at Γ ($m_{e\Gamma}$* =0.041).[45] However, since GeH can be thought of as hydrogen-terminated isolated (111) sheets of germanium, we are effectively eliminating the L wavevector in the Brillouin zone. We calculated from first-

principles[46,47] the phonon-limited electronic mobility for isolated single layer obtaining a high mobility of 18195 cm^2/Vs. This 5x increase in electron mobility from bulk Ge (3900 cm^2/Vs) is consistent with the reduced electron effective mass in GeH.

Also, using the EXCITING-CODE, we solved the Bethe-Salpeter equation to account for the excitonic effects.[48] We used the scissors operator to obtain a band gap of 1.53 eV for the two layer unit cell (to match our HSE calculated band gap value). Within this theoretical framework we calculated an excitonic binding energy of 0.28 eV for the two layer unit cell. Pulci *et al*.[49] used the GW approximation to calculate the ground state of germanane. They found a much larger direct quasi-particle band gap of 2.4 eV, far outside of the experimental range established here. They reported an excitonic peak with a higher binding energy of 0.6 eV below the conduction band. The difference between Pulci's exciton binding energy and our reported value agrees with the fact that our smaller band gap provides a larger screening that can decrease the exciton binding energy. No excitonic phenomena were observed in the absorption or photoluminescence of our samples. However, this 0.28 eV exciton binding energy may explain the previously observed 0.45 eV red shift between the absorption onset and photoluminescence of epitaxial GeH thin films.[32]

Chapter 6: Exfoliation of Single Layers

Finally, we demonstrate that hydrogen-terminated germanane can be mechanically exfoliated into single sheets. As with most other layered crystal structures, the GeH crystal structure is held together mainly *via* van der Waals bonding. By incorporating van der Waals corrections into the PBE simulation, the interlayer binding energy for GeH was found to be nearly entirely dominated by van der Waals interaction with a value of 72 meV per Ge atom, in the same range as the calculated 53.5 meV per C atom in graphite.[41] We therefore used both scotch tape and polydimethylsiloxane to exfoliate few and single layer thick sheets onto Si substrates with a wide range of SiO_2 thicknesses (100-165, 275-345 nm) to attain maximum contrast by optical microscopy. Few-layer and single-layer sheets were visible by optical microscopy, with 110 nm and 300 nm thick SiO_2 substrates providing optimal contrast. **Figure 11a** shows an AFM image, optical micrograph, and corresponding height profile for a 6-7 layer thick germanane flake. **Figure 11b** shows an AFM image, optical micrograph and the corresponding height profile for a 2 μm × 2 μm single GeH layer exfoliated onto a 100 nm thick SiO_2/Si substrate. The observed height (~6 Å) agrees well with the expected value of 5.5 Å for a single layer, since it is well known that differences in the attractive potentials between the AFM tip, the substrate, and the layered material often causes the measured AFM thickness to be larger than the expected value.[50] The weak Raman intensities of few layer GeH, the photothermal degradation at laser intensities above 40 kW/cm^2 and the overlap of the two E_2 and A_1 Raman modes with higher order silicon

substrate Raman modes prevents the collection of thickness-dependent Raman maps on conventional SiO_2/Si substrates. Regardless, our ability to produce single and few layer thick germanane sheets with > 2 μm length and width will enable further study of the layer dependence on the vibrational, optical, and electronic properties.

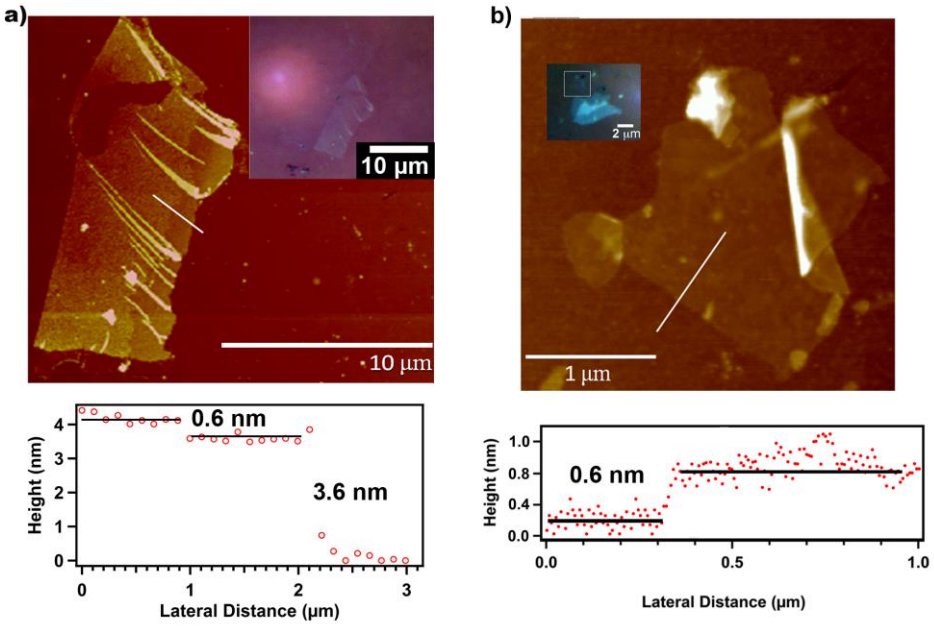

Figure 11. a) AFM micrograph (top), height profile (bottom), and optical micrograph (inset) of few layer GeH deposited on 110 nm SiO_2/Si. b) AFM micrograph (top), and height profile (bottom) of single layer thick GeH sheet.

Conclusion

In summary, we have created gram scale, mm-sized crystallites of hydrogen-terminated germanane and have characterized for the first time their long-term resistance to oxidation and thermal stability, a necessary prerequisite for any practical application. We have also demonstrated the ability to exfoliate single and few-layer sheets on surfaces, thus creating a germanium framework analogous to graphane. Theory predicts that the created material has a direct band gap of 1.55 eV with low effective masses, thus strongly increasing the already high carrier mobilities found in Ge without the penalty of the low bulk gap. This notion of creating dimensionally-reduced molecular-scale "allotropes" of materials with fundamentally different and potentially transformative properties compared to the bulk can be clearly expanded beyond carbon.

Methods

Synthesis

In a typical reaction, Ca and Ge were loaded in stoichiometric amounts into a quartz tube, and evacuated on a Schlenk line to millitorr pressures. The quartz tube was sealed under vacuum using a hydrogen-oxygen torch, and annealed at 950-1050 °C for 16-20 hours, and cooled to room temperature over 1-5 days. Germanium (Ge, 99.999%, Acros) and calcium (Ca, 99%, Acros) were purchased and used without further purification. To synthesize GeH, CaGe2 crystals were stirred in concentrated HCl (aq) for 5-10 days at -40 to -20 oC. To purify GeH, the GeH product was washed with milliQ H2O followed by methanol, then dried at room temperature on a Schlenk line.

Measurements

Powder x-ray diffraction was collected on a Bruker D8 powder x-ray diffractometer. FTIR and time dependent FTIR measurements were collected on a Perkin Elmer Frontier Dual-Range FIR/MidIR Spectrometer that was loaded in an Ar-filled glovebox. Raman scattering spectra was collected using a Renishaw InVia Raman equipped with a CCD detector. The Raman spectra were collected using 633 nm (He-Ne red laser) and 785 nm (near IR diode laser) illumination. XPS was collected using a Kratos Axis Ultra X-ray photoelectron spectrometer equipped with a monochromated (Al) X-ray gun. The Ar ion etch rate was calibrated using SiO_2. AFM images were collected on a Bruker 3000 scanning probe microscope with a

Nanoscope IIIa controller. X-ray fluorescence measurements were performed using an Olympus DELTA Handheld X-ray fluorescence Analyzer. TGA was performed using a TA instruments Q-500 Thermogravimetric Analyzer. Samples were analyzed from room temperature to 375 ^{o}C at a ramp rate of 10 ^{o}C/min under flowing N_2 atmosphere. Diffuse Reflectance Absorption measurements were conducted using a CARY 5000 UV/Vis NIR spectrophotometer, with a diffuse reflectance integrating sphere attachment.

References

(1) Novoselov, K. S.; Geim, A. K.; Morozov, S. V.; Jiang, D.; Katsnelson, M. I.; Grigorieva, I. V.; Dubonos, S. V.; Firsov, A. A. Two-Dimensional Gas of Massless Dirac Fermions in Graphene *Nature* **2005**, *438*, 197-200.
(2) Novoselov, K. S.; Geim, A. K.; Morozov, S. V.; Jiang, D.; Zhang, Y.; Dubonos, S. V.; Grigorieva, I. V.; Firsov, A. A. Electric Field Effect in Atomically Thin Carbon Films *Science* **2004**, *306*, 666-69.
(3) Fowler, J. D.; Allen, M. J.; Tung, V. C.; Yang, Y.; Kaner, R. B.; Weiller, B. H. Practical Chemical Sensors from Chemically Derived Graphene *ACS Nano* **2009**, *3*, 301-6.
(4) Liang, Y.; Li, Y.; Wang, H.; Zhou, J.; Wang, J.; Regier, T.; Dai, H. Co3O4 Nanocrystals on Graphene as a Synergistic Catalyst for Oxygen Reduction Reaction *Nat. Mater.* **2011**, *10*, 780-86.
(5) Williams, G.; Seger, B.; Kamat, P. V. TiO_2-Graphene Nanocomposites. UV-Assisted Photocatalytic Reduction of Graphene Oxide *ACS Nano* **2008**, *2*, 1487-91.
(6) Novoselov, K. S.; Jiang, D.; Schedin, F.; Booth, T. J.; Khotkevich, V. V.; Morozov, S. V.; Geim, A. K. Two-Dimensional Atomic Crystals *Proc. Nat. Acad. Sci.* **2005**, *102*, 10451-53.
(7) Ci, L.; Song, L.; Jin, C.; Jariwala, D.; Wu, D.; Li, Y.; Srivastava, A.; Wang, Z. F.; Storr, K.; Balicas, L.; Liu, F.; Ajayan, P. M. Atomic Layers of Hybridized Boron Nitride and Graphene Domains *Nat. Mater.* **2010**, *9*, 430-35.
(8) Lee, C.; Yan, H.; Brus, L. E.; Heinz, T. F.; Hone, J.; Ryu, S. Anomalous Lattice Vibrations of Single- and Few-Layer MoS_2 *ACS Nano* **2010**, *4*, 2695-700.
(9) Mak, K. F.; Lee, C.; Hone, J.; Shan, J.; Heinz, T. F. Atomically Thin MoS_2: A New Direct-Gap Semiconductor *Phys. Rev. Lett.* **2010**, *105*, 136805.
(10) Radisavljevic, B.; Radenovic, A.; Brivio, J.; Giacometti, V.; Kis, A. Single-layer MoS_2 Transistors *Nat. Nano.* **2011**, *6*, 147-50.
(11) Elias, D. C.; Nair, R. R.; Mohiuddin, T. M. G.; Morozov, S. V.; Blake, P.; Halsall, M. P.; Ferrari, A. C.; Boukhvalov, D. W.; Katsnelson, M. I.; Geim, A. K.; Novoselov, K. S. Control of Graphene's Properties by Reversible Hydrogenation: Evidence for Graphane *Science* **2009**, *323*, 610-13.
(12) Lomeda, J. R.; Doyle, C. D.; Kosynkin, D. V.; Hwang, W.-F.; Tour, J. M. Diazonium Functionalization of Surfactant-Wrapped Chemically Converted Graphene Sheets *J. Am. Chem. Soc.* **2008**, *130*, 16201-06.
(13) Becerril, H. A.; Mao, J.; Liu, Z.; Stoltenberg, R. M.; Bao, Z.; Chen, Y. Evaluation of Solution-Processed Reduced Graphene Oxide Films as Transparent Conductors *ACS Nano* **2008**, *2*, 463-70.
(14) Feng, B.; Ding, Z.; Meng, S.; Yao, Y.; He, X.; Cheng, P.; Chen, L.; Wu, K. Evidence of Silicene in Honeycomb Structures of Silicon on Ag(111) *Nano Lett.* **2012**, *12*, 3507-11.

(15) Lew Yan Voon, L. C.; Sandberg, E.; Aga, R. S.; Farajian, A. A. Hydrogen compounds of group-IV nanosheets *Appl. Phys. Lett.* **2010**, *97*, 163114/1-14/3.
(16) Ni, Z.; Liu, Q.; Tang, K.; Zheng, J.; Zhou, J.; Qin, R.; Gao, Z.; Yu, D.; Lu, J. Tunable Bandgap in Silicene and Germanene *Nano Lett.* **2012**, *12*, 113-18.
(17) O'Hare, A.; Kusmartsev, F. V.; Kugel, K. I. A Stable "Flat" Form of Two-Dimensional Crystals: Could Graphene, Silicene, Germanene Be Minigap Semiconductors? *Nano Lett.* **2012**, *12*, 1045-52.
(18) Vogg, G.; Brandt, M. S.; Stutzmann, M. Polygermyne - A Prototype System for Layered Germanium Polymers *Adv. Mater.* **2000**, *12*, 1278-81.
(19) Okamoto, H.; Kumai, Y.; Sugiyama, Y.; Mitsuoka, T.; Nakanishi, K.; Ohta, T.; Nozaki, H.; Yamaguchi, S.; Shirai, S.; Nakano, H. Silicon Nanosheets and Their Self-Assembled Regular Stacking Structure *J. Am. Chem. Soc.* **2010**, *132*, 2710-18.
(20) Dahn, J. R.; Way, B. M.; Fuller, E.; Tse, J. S. Structure of Siloxene and Layered Polysilane (Si_6H_6) *Phys. Rev. B* **1993**, *48*, 17872-7.
(21) Kautsky, H.; Herzberg, G. Concerning Siloxane and its Derivatives *Zeit. Anorg. Allgem. Chem.* **1924**, *139*, 135-60.
(22) Yamanaka, S.; Matsuura, H.; Ishikawa, M. New Deintercalation Reaction of Calcium from Calcium Disilicide. Synthesis of layered polysilane *Mater. Res. Bull.* **1996**, *31*, 307-16.
(23) Faessler, T. F. Germanium(cF136): A New Crystalline Modification of Germanium with the Porous Clathrate-II Structure *Angew. Chem. Int. Ed.* **2007**, *46*, 2572-75.
(24) Kiefer, F.; Karttunen, A. J.; Doblinger, M.; Fassler, T. F. Bulk Synthesis and Structure of a Microcrystalline Allotrope of Germanium (m-allo-Ge) *Chem. Mat.* **2011**, *23*, 4578-86.
(25) Bermejo, D.; Cardona, M. Infrared-Absorption in Hydrogenated Amorphous and Crystallized Germanium *J. Non-Cryst. Solids* **1979**, *32*, 421-30.
(26) Cardona, M. Vibrational-Spectra of Hydrogen in Silicon and Germanium *Phys. Stat. Solidi B* **1983**, *118*, 463-81.
(27) Rivillon, S.; Chabal, Y. J.; Amy, F.; Kahn, A. Hydrogen Passivation of Germanium (100) Surface Using Wet Chemical Preparation *Appl. Phys. Lett.* **2005**, *87*.
(28) Deegan, T.; Hughes, G. An X-ray Photoelectron Spectroscopy Study of the HF Etching of Native Oxides on Ge(111) and Ge(100) Surfaces *Appl. Surf. Sci.* **1998**, *123*, 66-70.
(29) Bodlaki, D.; Yamamoto, H.; Waldeck, D. H.; Borguet, E. Ambient Stability of Chemically Passivated Germanium Interfaces *Surf. Sci.* **2003**, *543*, 63-74.
(30) Lee, P. A.; Said, G.; Davis, R.; Lim, T. H. On Optical Properties of Some Layer Compounds *J. Phys. Chem. Solids* **1969**, *30*, 2719-29.
(31) Gaiser, C.; Zandt, T.; Krapf, A.; Serverin, R.; Janowitz, C.; Manzke, R. Band-gap Engineering with HfS_xSe_{2-x} *Phys. Rev. B* **2004**, *69*, 075205.
(32) Vogg, G.; Meyer, A. J. P.; Miesner, C.; Brandt, M. S.; Stutzmann, M. Efficient Tunable Luminescence of SiGe Alloy Sheet Polymers *Appl. Phys. Lett.* **2001**, *78*, 3956-58.
(33) Holman, Z. C.; Kortshagen, U. R. Nanocrystal Inks Without Ligands: Stable Colloids of Bare Germanium Nanocrystals *Nano Lett.* **2011**, *11*, 2133-36.

(34) Donovan, T. M.; Spicer, W. E.; Bennett, J. M. Evidence for a Sharp Absorption Edge in Amorphous Ge *Phys. Rev. Lett.* **1969**, *22*, 1058-61.
(35) Chambouleyron, I.; Graeff, C. F.; Zanatta, A. R.; Fajardo, F.; Mulato, M.; Campomanes, R.; Comedi, D.; Marques, F. C. The Perspectives of Hydrogenated Amorphous Germanium as an Electronic Material *Phys. Stat. Solidi B* **1995**, *192*, 241-51.
(36) Kresse, G.; Hafner, J. Ab initio Molecular-Dynamics for Liquid-Metals *Phys. Rev. B* **1993**, *47*, 558-61.
(37) Kresse, G.; Hafner, J. Ab Initio Molecular-Dynamics Simulation of the Liquid-Metal Amorphous-Semiconductor Transition in Germanium *Phys. Rev. B* **1994**, *49*, 14251-69.
(38) Blochl, P. E. Projector Augmented-Wave Method *Phys. Rev. B* **1994**, *50*, 17953-79.
(39) Perdew, J. P.; Burke, K.; Ernzerhof, M. Generalized Gradient Approximation Made Simple *Phys. Rev. Lett.* **1996**, *77*, 3865-68.
(40) Perdew, J. P.; Burke, K.; Ernzerhof, M. Generalized Gradient Approximation Made Simple *Phys. Rev. Lett.* **1997**, *78*, 1396.
(41) Grimme, S. Semiempirical GGA-type Density Functional Constructed with a Long-Range Dispersion Correction *J. Comp. Chem.* **2006**, *27*, 1787-99.
(42) Heyd, J.; Scuseria, G. E.; Ernzerhof, M. Hybrid Functionals Based on a Screened Coulomb Potential *J. Chem. Phys.* **2003**, *118*, 8207-15.
(43) Heyd, J.; Scuseria, G. E.; Ernzerhof, M. Hybrid Functionals Based on a Screened Coulomb Potential *J. Chem. Phys.* **2006**, *124*, 219906.
(44) Paier, J.; Marsman, M.; Hummer, K.; Kresse, G.; Gerber, I. C.; Angyan, J. G. Screened Hybrid Density Functionals Applied to Solids *J. Chem. Phys.* **2006**, *125*.
(45) *Landolt-Bornstein*; Madelung, O.; Schulz, M.; Weiss, H., Eds.; Springer: Berlin, 1987; Vol. 17a-h.
(46) Restrepo, O. D.; Varga, K.; Pantelides, S. T. First-Principles Calculations of Electron Mobilities in Silicon: Phonon and Coulomb Scattering *Appl. Phys. Lett.* **2009**, *94*, 212103.
(47) Baroni, S. *Quantum ESPRESSO* http://www.quantum-espresso.org/
(48) Sagmeister, S.; Ambrosch-Draxl, C. Time-dependent Density Functional Theory Versus Bethe-Salpeter Equation: an All-Electron Study *Phys. Chem. Chem. Phys.* **2009**, *11*, 4451-57.
(49) Pulci, O.; Gori, P.; Marsili, M.; Garbuio, V.; Del Sole, R.; Bechstedt, F. Strong Excitons in Novel Two-Dimensional Crystals: Silicane and Germanane *EPL* **2012**, *98*, 37004.
(50) Nemes-Incze, P.; Osvath, Z.; Kamaras, K.; Biro, L. P. Anomalies in Thickness Measurements of Graphene and Few Layer Graphite Crystals by Tapping Mode Atomic Force Microscopy *Carbon* **2008**, *46*, 1435-42.